Antimicrobial activity of poly(3,4-ethylenedioxythiophene) n-doped with a pyridinium-containing polyelectrolyte

Margarita Sánchez-Jiménez,[1,*] Francesc Estrany,[1,2] Núria Borràs,[1] Binoy Maiti,[3] David Díaz Díaz,[3,4] Luis J. del Valle,[1,2,*] Carlos Alemán[1,2,5,*]

[1] *Departament d'Enginyeria Química, EEBE, Universitat Politècnica de Catalunya, C/ Eduard Maristany, 10-14, Ed. I2, 08019, Barcelona, Spain*

[2] *Barcelona Research Center for Multiscale Science and Engineering, Universitat Politècnica de Catalunya, C/ Eduard Maristany, 10-14, Ed. C, 08019, Barcelona, Spain*

[3] *Institut für Organische Chemie, Universität Regensburg, Universitätsstr. 31, 93053 Regensburg, Germany*

[4] *Instituto de Productos Naturales y Agrobiología del CSIC, Avda. Astrofísico Francisco Sánchez 3, 38206 La Laguna, Tenerife, Spain*

[5] *Institute for Bioengineering of Catalonia (IBEC), The Barcelona Institute of Science and Technology, Baldiri Reixac 10-12, 08028 Barcelona Spain*

[*] Correspondence to: margarita.sanchez@upc.edu, luis.javier.del.valle@upc.edu and carlos.aleman@upc.edu

ABSTRACT

Poly(pyridinium-1,4-diyliminocarbonyl-1,4-phenylene-methylene chloride), abbreviated P(Py-1,4-P), has been used to prepare n-doped poly(3,4-ethylenedioxythiophene) (PEDOT) electrodes applying a reduction potential to a de-doped PEDOT film in a P(Py-1,4-P) water solution. The utilization of this cationic polyelectrolyte as n-dopant agent results in drastic superficial changes, as is observed by comparing the morphology, topography and wettability of p-doped, de-doped and n-doped PEDOT. Cytotoxicity, cell adhesion and cell proliferation assays, which have been conducted using epithelial and fibroblast cell lines, show that the amount of P(Py-1,4-P) in re-doped PEDOT films is below the one required to observe a cytotoxic harmful response and that n-doped PEDOT:P(Py-1,4-P) films are biocompatible. The non-specific bacteriostatic properties of n-doped PEDOT:P(Py-1,4-P) films has been demonstrated against *E. coli* and *S. aureus* bacteria (Gram-negative and Gram-positive, respectively) using bacterial growth curves and adhesion assays. Although the bacteriostatic effect is in part due to the conducting polymer, as is proved by results for p-doped and de-doped PEDOT, the incorporation of P(Py-1,4-P) through the re-doping process greatly enhances this antimicrobial behaviour. Thus, only a small concentration of this cationic polyelectrolyte (~0.1 mM) is needed to inhibit bacterial growth.

INTRODUCTION

The utilization of polyelectrolytes as dopant anions of conducting polymers (CPs) is a frequent approach. A well-known example is the preparation of p-doped poly(3,4-ethylenedioxythiophene) (PEDOT; Scheme 1), which is one of the most studied CPs because of its excellent properties (*i.e.* great environmental stability, electrical conductivity, electrochemical activity, thermoelectric behaviour and high specific capacitance),[1-6] using poly(styrenesulfonate) (PSS).[7-14] The PEDOT:PSS complex consists of a phase segregated structure in which ~30 nm diameter conductive PEDOT-rich polycationic domains are encapsulated by ~1 nm thick PSS-rich polyanionic shells.[7] The CP domains are embedded in an electronically insulating PSS matrix loosely cross-linked by hydrogen bonding.[8] PSS-doped PEDOT polymer mixtures exhibit good film forming properties, moderate to high conductivity, high visible light transmittance and excellent stability and, therefore, are suitable for use as low-cost wearable sensors,[9] electrodes for supercapacitors,[10-12] soft actuators,[13,14] and as hole injection/extraction material in organic optoelectronics,[15] among others.

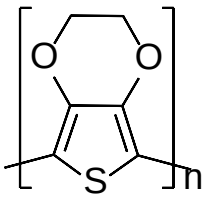

Scheme 1. Chemical structure of PEDOT

In spite of the literature about p-doped PEDOT obtained using polyanionic dopants is very abundant, the number of studies on n-doped PEDOT prepared with polycations is very scarce.[16,17] This is amazing since PEDOT is one of the few CPs that are both p- and n-dopable, as was shown by Inganäs and co-workers more than two decades ago.[15] Indeed, the few studies reported on negatively charged PEDOT have been focussed on

the spectroscopic, electrical and electrochemical properties of the polymer doped with small tetra-alkylammonium cations[18-21] and imidazolium-containing ionic liquids.[22] In very recent studies, we proposed the preparation of anodically polymerized PEDOT n-doped with cationic polyelectrolytes bearing quaternary ammonium.[16,17] More specifically, we used three ionene polymers containing 1,4-diazabicyclo[2.2.2]octane (DABCO) and N,N'-(*x*-phenylene)dibenzamide (*x*= *ortho*- / *meta*- / *para*-), which exhibited different gelation capacity in aqueous media,[23,24] as macromolecular dopant agents. Interestingly, n-doped PEDOT films obtained using such DABCO-based ionenes exhibited a noticeable improvement of the mechanical response, thermal stability and specific capacitance, with respect to those prepared using conventional tetramethylammonium.[16,17]

In this work we have extended the utilization of cationic polyelectrolytes to provide biocompatible n-doped PEDOT electrodes with antibacterial activity. More specifically, we have used poly(pyridinium-1,4-diyliminocarbonyl-1,4-phenylene-methylene chloride), hereafter denoted P(Py-1,4-P) (Scheme 2), an ionic gelator firstly reported by Yoshida and coworkers one decade ago[25] that is applicable to a broad range of solvents (*i.e.* organic and aqueous) by anion-exchange reaction. Furthermore, Kundu *et al.*[26] studied the structural parameters of these polyelectrolyte in dilute aqueous solutions far below the gelation threshold, in the sol state and after gelation using static/dynamic light scattering and small-angle neutron scattering. Gelation of multifucntional P(Py-1,4-P) was attributed through hydrogen bonding, π–π interactions, ion–π interactions and electrostatic interactions relating to the polyelectrolyte effect.[27]

It is worth noting that the antimicrobial properties of polymers containing pyridinium halides like quaternary nitrogen salts are well known.[28-32] The antimicrobial activity of these polyelectrolytes depends on the adsorptive activities on the surface of bacterial

cells as well as their destruction and the pKa values of the corresponding pyridines, while factors controlling their antimicrobial activity are molecular hydrophobicity, adsorbability, surface activity and electron density of the ammonium nitrogen atom.[28-33] Therefore, PEDOT films reduced with P(Py-1,4-P) are potential candidates to behave not only as n-doped electrodes, but also as efficient antimicrobial materials for bioelectronic applications. For this purpose, p-doped PEDOT films have been de-doped in aqueous medium and subsequently re-doped in presence of P(Py-1,4-P) aqueous solutions by applying a reduction potential. The structural, morphological and electrochemical properties of the resulting films, hereafter PEDOT:P(Py-1,4-P), have been characterized. After this, the cytotoxicity of the polycation and the biocompatibility of n-doped PEDOT:P(Py-1,4-P) have been examined considering epithelial and fibroblast cells. Finally, the antimicrobial activity of n-doped PEDOT:P(Py-1,4-P) has been examined and compared with that of p-doped and de-doped PEDOT using growth inhibition and adhesion experiments with *E. coli* and *S. aureus*.

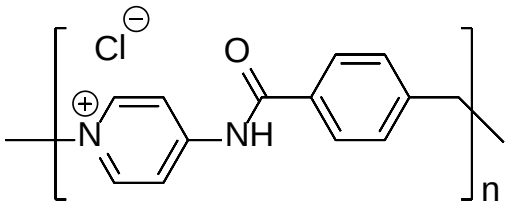

Scheme 2. Chemical structure of P(Py-1,4-P).

RESULTS AND DISCUSSION

Preparation and characterization

PEDOT was electropolymerized onto steel AISI 316 electrodes (2 cm^2) using a 10 mM monomer solution in acetonitrile with 100 mM $LiClO_4$, as supporting electrolyte, and applying a constant potential of +1.40 V until a polymerization charge of 480

mC/cm^2 was reached. The resulting p-doped PEDOT:ClO_4^- films were de-doped applying a potential of –1.50 V during 120 s in a 10 mM $LiClO_4$ acetonitrile solution. Finally, de-doped PEDOT films were n-doped by chronoamperometry, applying a constant reduction potential during 300 s, in a 10 mM P(Py-1,4-P) aqueous solutions. Four reduction potentials (*i.e.* –0.50, –0.70, –0.90 and –1.10 V) were initially tested, the highest electrochemical activity being obtained for –1.10 V. This is reflected in Figure 1a, which compares the control voltammograms of n-doped films prepared using the different reduction potentials. The electrochemical activity, which corresponds to the similarity between the cathodic and anodic areas, increases with decreasing reduction potential. The same feature is derived from Figure 1b, which represents the variation of the charge passed through the PEDOT:P(Py-1,4-P) films against the reduction potential. Overall, results indicate that the ability of PEDOT:P(Py-1,4-P) films to exchange charge reversibly improves significantly when the reduction potential is –1.10 V.

Figure 1c represents the variation of the doping level (*DL*) for the materials prepared using different reduction potentials against the number of consecutive oxidation and reduction cycles (*N*). In this work the *DL* was expressed as:

$$DL = \frac{Q_{nd-N}}{Q_g - Q_d} \times 100 \qquad (1)$$

where $Q_{nd\text{-}N}$ is the charge of PEDOT:P(Py-1,4-P) films in the redox cycle *N*, Q_g is the charge consumed during the polymerization process of p-doped PEDOT films and Q_d is the charge consumed during the de-doping process for elimination of ClO_4^- counterions. The *DL* and, therefore, the incorporation of P(Py-1,4-P) molecules into the PEDOT matrix during the re-doping process increase with decreasing reduction potential. Furthermore, the *DL* decreases with increasing number of redox cycles in all cases, which has been attributed to the structural changes caused in the CP matrix by the

electrochemical reactions. Due to these changes, all the P(Py-1,4-P) molecules that escape from the PEDOT matrix upon oxidation are not able to re-enter when the next reduction scan is applied. However, the *DL* almost reaches a steady state after 15 redox cycles, showing the structural stabilization of the PEDOT matrix. Interestingly, the difference between the *DL* reached at –1.10 V and those obtained at higher reduction potentials increases with the number of redox cycles, confirming that the former is the most appropriated.

In order to compare the role of P(Py-1,4-P) polyelectrolyte with conventional tetramethylammonium (TMA) as reducing agent, n-doped PEDOT:TMA films were prepared using the same approach and applying –0.50, –0.70, –0.90 and –1.10 V as reduction potentials. The variation of the *DL* for the obtained films against the number of redox cycles is displayed in Figure 1d. As expected, for each reduction potential the *DL* is higher for films re-doped with TMA than with P(Py-1,4-P). Moreover, the *DL*s obtained for films re-doped at –0.90 and –1.10 V are practically identical. Obviously, the higher n-doping capacity of TMA has been associated to the mobility of this small cation, which is greater than that of the cationic polyelectrolytes.

In order to get more information about n-doped PEDOT:P(Py-1,4-P) films obtained at –1.10 V, p-doped PEDOT:ClO_4^- films were obtained using different polymerization times and subsequently de-doped and re-doped with P(Py-1,4-P) using the above described conditions. The charge after de-doping and re-doping at –1.10 V, *Q* (in C), was calculated on each voltammogram. Figure 1e, which represents the film weight *m* against *Q*, provides linear profiles with a correlation coefficient higher than 0.97 for both de-doping and re-doping processes, reflecting their Faradic behaviour. Moreover, the *Q* is higher for re-doped films than for de-doped ones when similar *m* values are compared, corroborating the incorporation of the negatively charged polyelectrolyte.

Figure 2a compares the FTIR spectra recorded for p-doped PEDOT, de-doped PEDOT and n-doped PEDOT:P(Py-1,4-P). The FTIR fingerprints of PEDOT were discussed in previous work[16,17] and, therefore, we have focused on the identification of the P(Py-1,4-P) characteristic bands associated to the –CONH– bonds. The successful incorporation of the polyelectrolyte is clearly evidenced by the apparition of the sharp peaks at 1683, 1513 and 1204 cm^{-1}, which correspond to the amide I, amide II and amide III, respectively, and the broad shoulders at 3370 and 3021 cm^{-1} that has been attributed to the amide A and amide B, respectively.

The surface morphology of p-doped PEDOT, de-doped PEDOT and PEDOT:P(Py-1,4-P) was investigated by scanning electron microscopy (SEM). As shown in Figure 3, low magnification micrographs indicate that the surface structure of p-doped PEDOT, exhibits a dense and relatively uniform distribution of cauliflower shaped clusters (*i.e.* clusters of similar sizes with a few exceptions). This morphology becomes more open after de-doping. Thus, the structure of de-doped PEDOT can be defined as a distribution of large clusters very separated among them and surrounded by smaller clusters. Finally, n-doping with P(Py-1,4-P) results in a re-structuration, originating a very uniform distribution of clusters that are smaller than those found for p-doped and de-doped PEDOT. These differences are clearly reflected in representative high magnification SEM micrographs (Figure 3), which also show that the surface porosity is higher for PEDOT:P(Py-1,4-P) than for p-doped and de-doped PEDOT. Besides, SEM micrographs obtained for PEDOT:TMA, which are included in Figure 3, show a surface morphology similar to that of PEDOT:P(Py-1,4-P). This result indicates that, apparently, the structure of the n-doped CP is not affected by the chemical structure of the dopant agent.

As shown in Figures 4, 3D topographic and 2D height AFM images, which include the values of the arithmetic average roughness (R_a) and the root mean square roughness (R_q), are fully consistent with SEM micrographs. The surface roughness and the average size of the cluster decrease progressively after de-doping and re-doping. Furthermore, height AFM images clearly show that the surface porosity is higher for PEDOT:P(Py-1,4-P) than for de-doped and, especially, p-doped PEDOT. Moreover, the topographic characteristic of PEDOT:TMA (Figure S2) are similar to those of PEDOT:P(Py-1,4-P), even though the reduction in the size of the clusters and the increment in the surface porosity is less pronounced in the former than in the latter.

Contact angle (θ) measurements were performed to examine the influence of P(Py-1,4-P) in the wettability of the CP. Results displayed in Figure 2b reflect that the hydrophilicity of p-PEDOT increases upon de-doping (*i.e.* θ decreases from 63º±6º to 52º±5º), which is in agreement with previous observations and was attributed to the drastic change in the surface topography.[16] Incorporation of P(Py-1,4-P) results in a significant increment of the hydrophilicity, θ decreasing from 47º±5º to 31º±3º when the reduction potential varies from –0.50 to –1.10 V. Thus, the affinity of PEDOT:P(Py-1,4-P) films towards water increases with the amount of polyelectrolyte (*i.e.* with the doping level). In opposition, re-doping with TMA resulted in a hydrophobic material (θ= 98º±9º), which has been associated to the formation of a highly hydrophobic TMA layer at the surface of the films. This small organic molecule was found to act not only as n-dopant agent but also as organic coating.

Cytotoxicity and biocompatibility

The cytotoxicity of P(Py-1,4-P) and the biocompatibility of PEDOT:P(Py-1,4-P) is an important characteristic to be analysed for further biological applications. Both p-

doped PEDOT and de-doped PEDOT do not exhibit any toxic effect until they are used at very high concentrations, as it was already reported.[34,35] In this work the cytotoxicity of P(Py-1,4-P) alone has been tested in normal rat kidney fibroblast cells (NRK) and African green monkey kidney epithelial cells (VERO) using the MTT assay measured after 24 h post-treatment (Figure 5a). Although P(Py-1,4-P) showed cytotoxic effects for both cell lines, the amount of polyelectrolyte required to observe such harmful response is much higher than its concentration in the n-doped CP. More specifically, the concentration of P(Py-1,4-P) required to kill half the cells in the culture (CC_{50}) is 3.8 mM while no toxicity is detectable when the concentration is lower than 0.625 mM.

The adhesion (24 hours) and proliferation (7 days) of NRK fibroblast and VERO epithelial cells onto p-doped PEDOT, de-doped PEDOT, n-doped PEDOT:P(Py-1,4-P) and tissue culture polystyrene (TCPS) plates, which were used as a control, were evaluated to confirm the biocompatibility of the materials. Results for adhesion and proliferation are represented in Figures 5b and 5c, respectively. As it can be seen, the cellular adhesion onto p-doped, de-doped and n-doped films is comparable to that achieved for the control, independently of the cell line. Moreover, the number of viable cells on the surface of all the evaluated systems increases after 7 days. Results show that cell proliferation onto PEDOT:P(Py-1,4-P) films is comparable to the TCPS control, evidencing that the amount of polyelectrolyte loaded into n-doped films do not have a cytotoxic effect.

Bacterial growth

The antimicrobial activity of the P(Py-1,4-P) polyelectrolyte, acting as n-dopant agent of PEDOT, was assessed by quantitative measurement of the inhibition of

bacterial growth in broth. *Escherichia coli* (*E. coli*) and *Staphylococcus aureus* (*S. aureus*), which are Gram-negative and Gram-positive bacteria, respectively, were selected to evaluate the bacterial growth during 28 hours in contact with the p-doped, de-doped and n-doped PEDOT. The resulting bacterial growth curves, which are displayed in Figure 6, reflect the typical growth dynamics for both the vials without any film inside (control samples) and the samples containing CP films with different doping levels. Thus, curves show the initial lag phase (first 4 h), the exponential growth or logarithmic phase (up to ~20 h), and finally the stationary phase that lasts up to the end of the assay. The maximum bacterial growth after 28 h, which was established in relation to the control (100%), ranged from 73% to 61% and was mostly dependent on the doping level of the CP. More specifically, the system that provided the highest bacterial growth was the p-doped (73% for both bacteria), followed by the de-doped (69% for both bacteria), while PEDOT:P(Py-1,4-P) provided the lowest bacterial growth after 28 h (65% and 61% for *E. coli* and *S. aureus*, respectively). According to these results, PEDOT produced in the conditions reported in this work apparently hinders the growth of Gram-positive and Gram-negative bacteria, independently of the doping level. Moreover, the inhibition of the bacterial growth, which is very similar for p-doped and de-doped PEDOT films, increases by incorporating P(Py-1,4-P) through the re-doping process.

Quantification of bacterial adhesion is another checkpoint of bactericide activity (Figure 7). This activity is clearly demonstrated for de-doped PEDOT and n-doped PEDOT:P(Py-14-P) films since the percentage of bacteria adhered on their surface was always statistically lower than that on the control. In fact, bacterial adhesion tests show that n-doped films exhibit the highest bacteriostatic effect, which has been attributed to the antimicrobial properties of the P(Py-1,4-P). In order to corroborate this hypothesis,

the antimicrobial behaviour of the P(Py-1,4-P) was examined by evaluating the bacterial growth as function of the polyelectrolyte concentration.

Bacterial growth curves (48 h) displayed in Figure 8 reveal that the bacteriostatic effect of P(Py-1,4-P) increases rapidly with its concentration. Although the growth of the two bacteria decreases rapidly with increasing P(Py-1,4-P) concentration, the shape of the curves suggests that *S. aureus* is slightly more sensitive than *E. coli* to the polyelectrolyte concentration. In order to clarify this feature, the variation of the bacterial growing as a function of the concentration of P(Py-1,4-P) (in mM) was adjusted to the following linear Eqns for *E. coli* (Eqn 1) and *S. aureus* (Eqn 2):

$$\text{Ln (bacterial growth)} = -11.26 \cdot [\text{P(Py-1,4-P)}] + 4.65 \quad (R^2 = 0.989) \qquad (1)$$

$$\text{Ln (bacterial growth)} = -10.60 \cdot [\text{P(Py-1,4-P)}] + 4.34 \quad (R^2 = 0.998) \qquad (2)$$

Although the coefficient corresponding to the decay of bacterial growth is slightly higher for *S. aureus* than for *E. coli*, from a practical point of view both values are very similar. This observation is fully consistent with results displayed in Figures 6 and 7, which indicated that the sensitivity of *E. coli* and *S. aureus* to n-doped PEDOT:P(Py-1,4-P) films was indistinguishable. On the other hand, results displayed in Figure 8 indicate that the cytotoxic effects of P(Py-1,4-P) are more pronounced for bacteria than for eukaryotic cells. Thus, the minimum concentration of P(Py-1,4-P) required to kill NRK and VERO cells was higher than 0.625 mM (Figure 5), while a concentration of 0.156 mM affects considerably to the growth of *E. coli* and *S. aureus*.

CONCLUSIONS

The utilization of P(Py-1,4-P) as reducing agent for the preparation of n-doped PEDOT:P(Py-1,4-P) electrodes has been proved. These electrodes has been obtained by

de-doping previously synthesized p-doped PEDOT:ClO_4^- films and, subsequently, re-doping in presence of a P(Py-1,4-P) aqueous solution. The optimum re-doping potential, which provides the highest electrochemical activity and doping level, has been found to be –1.10 V. Although the new electrodes present morphological and electrochemical properties comparable to those obtained re-doping with conventional TMA, the chemical structure of P(Py-1,4-P) favours a new functionality. Thus, PEDOT:P(Py-1,4-P) electrodes have been found to exhibit significant antimicrobial properties. Bacterial growth and adhesion assays revealed that the incorporation of P(Py-1,4-P) enhances the bacteriostatic behaviour of PEDOT. Thus, although both p-doped and de-doped PEDOT films inhibit the bacterial growth, the bacteriostatic effect increases when a very small of P(Py-1,4-P) is incorporated into the CP matrix through the re-doping potential. Interestingly, P(Py-1,4-P) affects more bacteria than eukaryotic cells. Thus, no toxicity has been detected for NRK and VERO cells for P(Py-1,4-P) concentrations lower than 0.625 mM, whereas a concentration of 0.156 mM largely affects the growth of both Gram-positive and Gram-negative bacteria. Moreover, PEDOT:P(Py-1,4-P) shows a biocompatibility comparable to that of TCPS (control) while the unspecific bacteriostatic behaviour is maintained. In summary, biocompatible PEDOT:P(Py-1,4-P) electrodes exhibit and clear preventive effect against bacterial colonization and, therefore, are potential candidates to be evaluated as implantable electrodes for biomedical applications (*e.g.* regulation of drug delivery and tissue regeneration by electro-stimulation).

CONFLICTS OF INTEREST

There are no conflicts of interest to declare

ACKNOWLEDGEMENTS

Authors acknowledge MINECO/FEDER (RTI2018-098951-B-I00 and RTI2018-101827-B-I00), the Agència de Gestió d'Ajuts Universitaris i de Recerca (2017SGR359 and 2017SGR373). Support for the research of C.A. was received through the prize "ICREA Academia" for excellence in research funded by the Generalitat de Catalunya.

REFERENCES

1. O. Bubnova, Z. U. Khan, H. Wang, S. Braun, D. R. Evans, M. Fabretto, P. Hojati-Talemi, D. Dagnelund, J. B. Arlin, Y. H. Geerts, S. Desbief, D. W. Breiby, J. W. Andreasen, R. Lazzaroni, W. M. Chen, I. Zozoulenko, M. Fahlman, P. J. Murphy, M. Berggren and X. Crispin, *Nat. Mater.*, 2014, **13**, 190.
2. L. V. Kayser and D. J. Lipomi, *Adv. Mater.*, 2019, **31**, 1806133.
3. L. D. Sappia, E. Piccinini, W. Marmisolle, N. Santilli, E. Maza, S. Moya, F. Battaglini, R. E. Madrid and O. Azzaroni, *Adv. Mater. Interf.*, 2017, **17**, 1700502.
4. L. B. Groenendaal, F. Jonas, D. Freitag, H. Pielartzik and J. R. Reynolds, *Adv. Mater.*, 2000, **12**, 481.
5. D. Aradilla, F. Estrany and C. Alemán, *J. Phys. Chem. C*, 2011, **115**, 8430.
6. Q. Wei, M. Mukaida, K. Kirihara, Y. Naitoh and T. Ishida, *Materials*, 2015, **8**, 732.
7. U. Lang, N. Naujoks and J. Dual, *Synth. Met.*, 2009, **159**, 473.
8. T. Stöcker, A. Köhler and R. Moos, *J. Polym. Sci., Part B: Polym. Phys.*, 2012, **50**, 976.
9. M. Kuş and S. Okur, *Sens. Actuators B*, 2009, **143**, 177.
10. J. E. Lim, S. M. Lee, S. S. Kim, T. W. Kim, H. W. Koo and H. Kim, *Sci. Rep.*, 2017, **7**, 14685.

11. M. Y. Teo, N. Kim, S. Kee, B. S. Kim, G. Kim, S. Hong, S. Jung and K. Lee, *ACS Appl. Mater. Inferfaces*, 2017, **9**, 819.
12. G. F. Cai, P. Darmawan, M. Q. Cui, J. X. Wang, J. W. Chen, S. Magdassi and P. S. Lee, *Adv. Energy Mater.*, 2016, **6**, 1501882.
13. S. Taccola, F. Greco, E. Sinibaldi, A. Mondini, B. Mazzolai and V. Mattoli, *Adv. Mater.*, 2015, **27**, 1668.
14. Y. Li, M. Liu, Y. Li, K. Yuan, L. Xu, W. Yu, R. Chen, X. Qiu and H.-L. Yip, *Adv. Energy Mater.*, 2017, **7**, 1601499.
15. Q. B. Pei, G. Zuccarello, M. Ahlskog and O. Inganäs, *Polymer*, 1994, **35**, 1347.
16. M. G. Saborio, O. Bertran, S. Lanzalaco, M. Häring, D. D. Díaz, F. Estrany and C. Alemán, *Phys. Chem. Chem. Phys.*, 2018, **20**, 9855.
17. M. G. Saborio, O. Bertran, S. Lanzalaco, M. Häring, L. Franco, J. Puiggalí, D. Díaz Díaz, F. Estrany and C. Alemán, *Soft Matter*, 2018, **14**, 6374.
18. H. J. Ahonen, J. Lukkari and J. Kankare, *Macromolecules*, 2000, **33**, 6787.
19. M. Skompska, J. Mieczkowski, R. Holze and J. Heinze, *J. Electroanal. Chem.*, 2005, **577**, 9.
20. A. R. Hillman, S. J. Daisley and S. Bruckenstein, *Electrochim. Acta*, 2008, **53**, 3763.
21. H. Gustafsson, C. Kwarnström and A. Ivaska, *Thin Solid Films*, 2008, **517**, 474.
22. A. P. Sandoval, J. M. Feliu, R. Torresi and M. F. Suárez, *RSC Adv.*, 2014, **4**, 3383.
23. J. Bachl, D. Zanuy, D. E. López-Pérez, G. Revilla-López, C. Cativiela, C. Alemán and D. D. Diaz, *Adv. Funct. Mater.*, 2014, **24**, 4893.
24. J. Bachl, O. Bertran, J. Mayr, C. Alemán and D. D. Díaz, *Soft Matter*, 2017, **13**, 3031.

25. M Yoshida, N. Koumura, Y. Misawa, N. Tamaoki, H. Matsumoto, H. Kawanami, S. Kazaoui and N. Minami, *J. Am. Chem. Soc.*, 2007, **129**, 11039.

26. **S**. Kumar Kundu, N. Osaka, T. Matsunaga, M. Yoshida and M. Shibayama, *J. Phys. Chem. B*, 2008, **112**, 16469.

27. M. Suzuki and K. Hanabusa, *Chem. Soc. Rev.*, 2010, **39**, 455.

28. L. D. Li, X. F. Chi, F. Y. Gai, H. Zhou, F. X. Zhang and Z. B. Zhao, *J. Appl. Polym. Sci.*, 2017, **134**, 45323.

29. H. Yan, Z. D. Rengert, A. W. Thomas, C. Rehermann, J. Hinks, G. C. Bazan, Influence of molecular structure on the antimicrobial function of phenylenevinylene conjugated oligoelectrolytes. *Chem. Sci.*, 2016, **7**, 5714.

30. Y. Xue and H. Xiao, *Polymers*, 2015, **7**, 2290.

31. A. Jain, L. S. Duvvuri, S. Farah, N. Beyth, A. J. Domb and W. Khan, *Adv. Healthc. Mater.*, 2014, **3**, 1969.

32. F. Siedenbiedel, A. Fuchs, T. Moll, M. Weide, R. Breves and J. C. Tiller, *Macromol. Biosci.*, 2013, **13**, 1447.

33. T. R. Stratton, J. L. Rickus and J. P. Youngblood, *Biomacromolecules*, 2009, **10**, 2550.

34. A. Puiggalí-Jou, P. Micheletti, F. Estrany, L. J. del Valle and C. Alemán, *Adv. Healthcare Mater.*, 2017, **6,** 1700453.

35. L. J. del Valle, F. Estrany, E. Armelin, R. Oliver and C. Alemán, *Macromol. Biosci.*, 2008, **8**, 1144.

CAPTIONS TO FIGURES

Figure 1. (a) Control voltammograms registered at 25 ºC in a 10 mM P(Py-1,4-P) aqueous solution for n-doped PEDOT:P(Py-1,4-P) films prepared using different reduction potentials. (b) Variation of the voltammetric charge passed through the film in a 10 mM P(Py-1,4-P) aqueous solution against the reduction potential used in the re-doping process. Variation of the doping level (*DL*) for the (c) PEDOT:P(Py-1,4-P) and (d) PEDOT:TMA films re-doped using different reduction potentials against the number of consecutive oxidation and reduction cycles (*N*). (d) Film weight (*m*) against *Q* for PEDOT films after de-doping (red) and after re-doping with P(Py-1,4-P) (black).

Figure 2. (a) FTIR spectra of p-doped PEDOT, de-doped PEDOT and n-doped PEDOT:P(Py-1,4-P) obtained using a reduction potential of –1.10 V. (b) Contact angle of p-doped PEDOT, de-doped PEDOT and n-doped PEDOT:P(Py-1,4-P) obtained using different reduction potentials.

Figure 3. Low and high magnification SEM micrographs (left and right, respectively) of p-doped PEDOT, de-doped PEDOT, n-doped PEDOT:P(Py-1,4-P) and n-doped PEDOT:TMA.

Figure 4. 3D Topographic and 2D height AFM images (20×20 μm^2) of p-doped PEDOT, de-doped PEDOT and PEDOT:P(Py-1,4-P). Values of R_a and R_q are also displayed.

Figure 5. (a) Cytotoxicity of P(Py-1,4-P) on NRK and VERO cells for 24 h. (b) Cellular adhesion and (c) cellular proliferation on p-doped PEDOT, de-doped PEDOT and n-doped PEDOT:P(Py-1,4-P) films. Assays were performed using two representative eukaryotic cell lines (NRK and VERO). Three samples were analysed for each group. Bars represent the mean standard deviation. The relative viability was established in relation to the control (100%), which was TCPS.

Figure 6. Growth curves of the (a) *E. coli* and (b) *S. aureus* bacteria in the culture medium alone (control) and in presence of p-doped PEDOT, de-doped PEDOT and n-doped PEDOT:P(Py-1,4-P) films.

Figure 7. *E. coli* and *S. aureus* adhesion on TCPS (positive control) and in of p-doped PEDOT, de-doped PEDOT and n-doped PEDOT:P(Py-1,4-P) films. Bars represent the mean standard deviation. The relative viability of *E. coli* and *S. aureus* was established in relation to TCPS.

Figure 8. Growth curves of the (a) *E. coli* and (b) *S. aureus* bacteria in the culture medium alone (0.000 mM, which is the control) and in presence of different P(Py-1,4-P) concentrations.

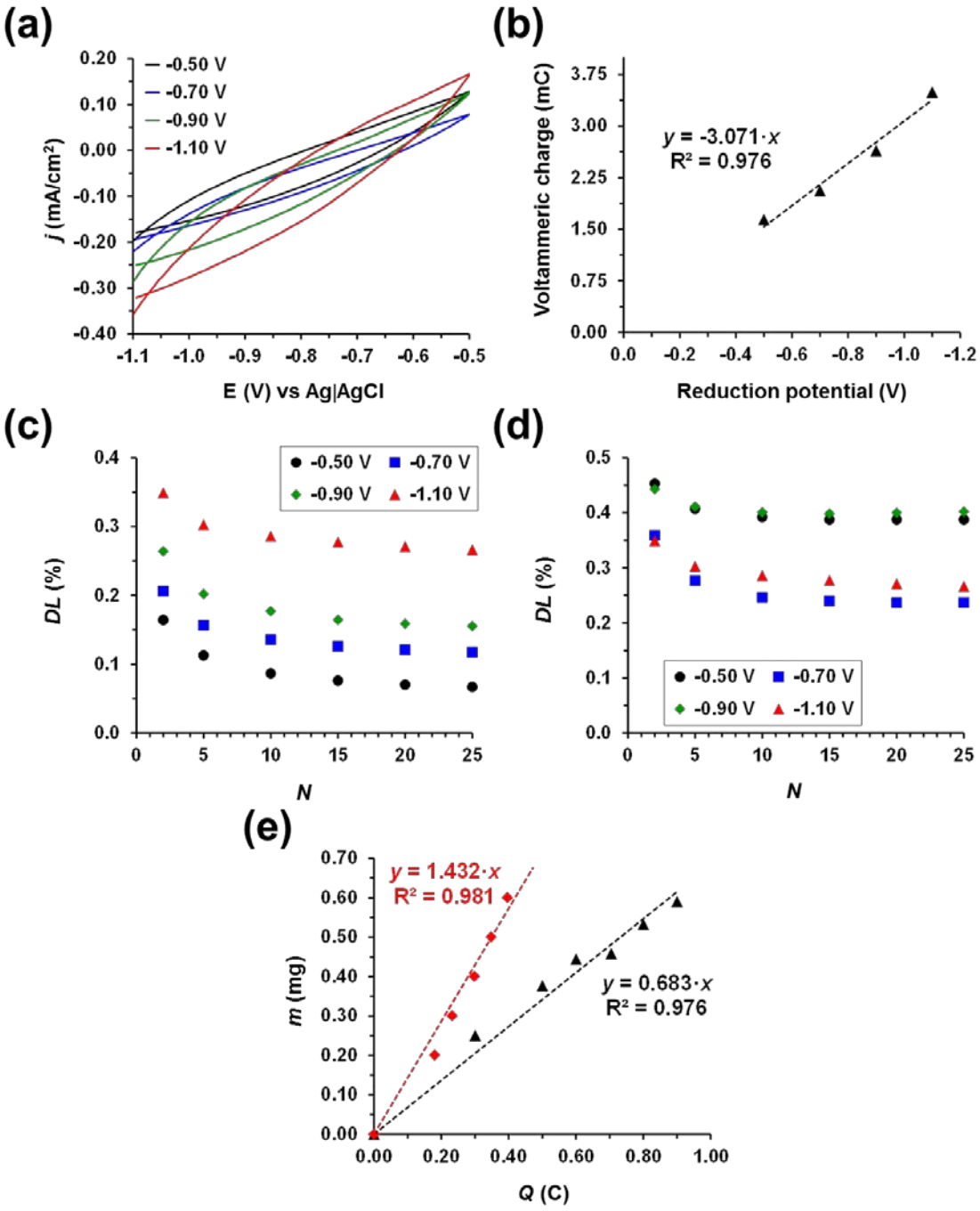
(a)
-0.50 V
-0.70 V
-0.90 V
-1.10 V
j (mA/cm²)
E (V) vs Ag|AgCl
(b)
y = -3.071·x
R² = 0.976
Voltammeric charge (mC)
Reduction potential (V)
(c)
-0.50 V
-0.70 V
-0.90 V
-1.10 V
DL (%)
N
(d)
-0.50 V
-0.70 V
-0.90 V
-1.10 V
DL (%)
N
(e)
y = 1.432·x
R² = 0.981
y = 0.683·x
R² = 0.976
m (mg)
Q (C)

Figure 1

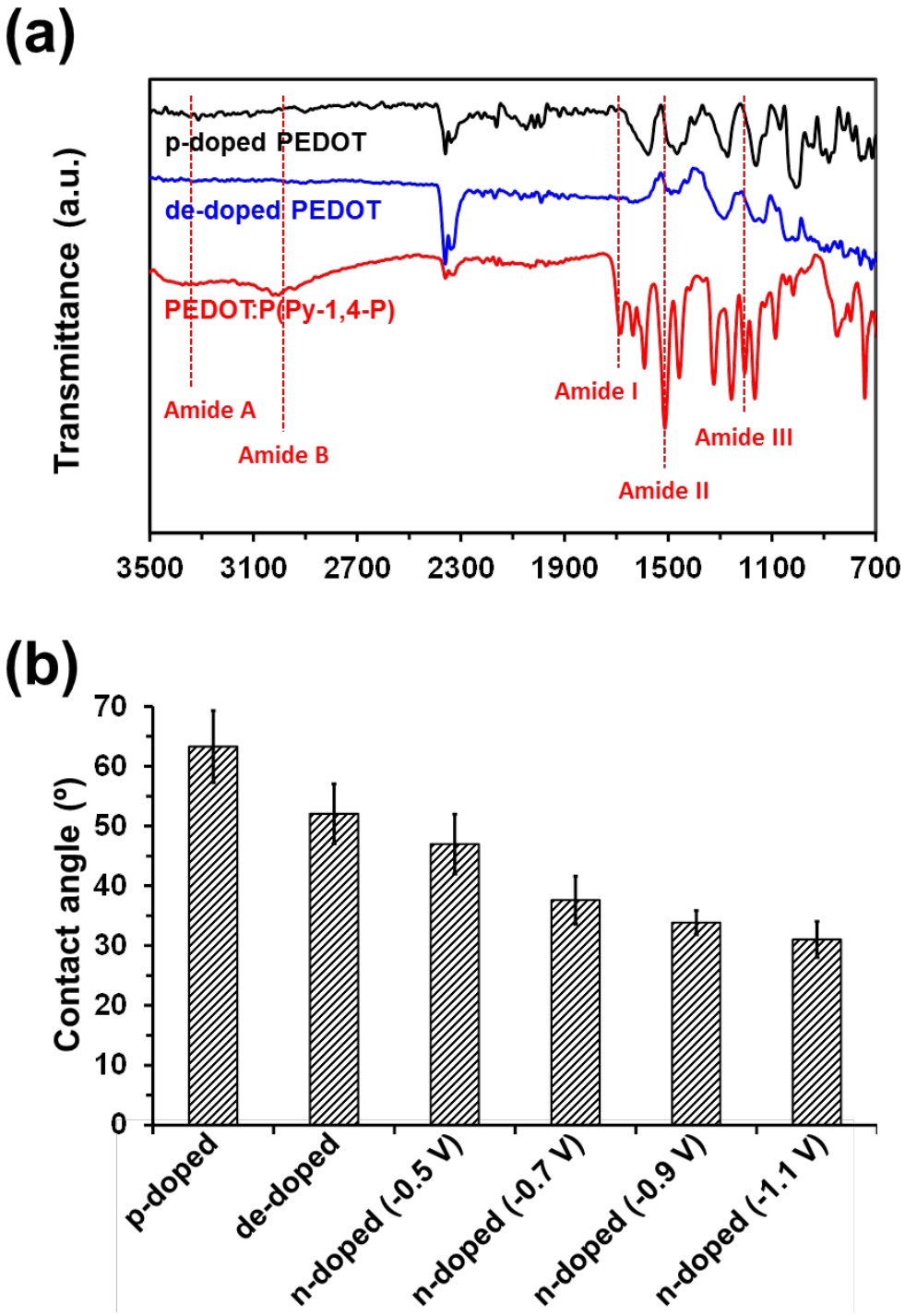
(a)
Transmittance (a.u.)
p-doped PEDOT
de-doped PEDOT
PEDOT:P(Py-1,4-P)
Amide A
Amide B
Amide I
Amide II
Amide III
3500
3100
2700
2300
1900
1500
1100
700
(b)
Contact angle (°)
70
60
50
40
30
20
10
0
p-doped
de-doped
n-doped (-0.5 V)
n-doped (-0.7 V)
n-doped (-0.9 V)
n-doped (-1.1 V)

Figure 2

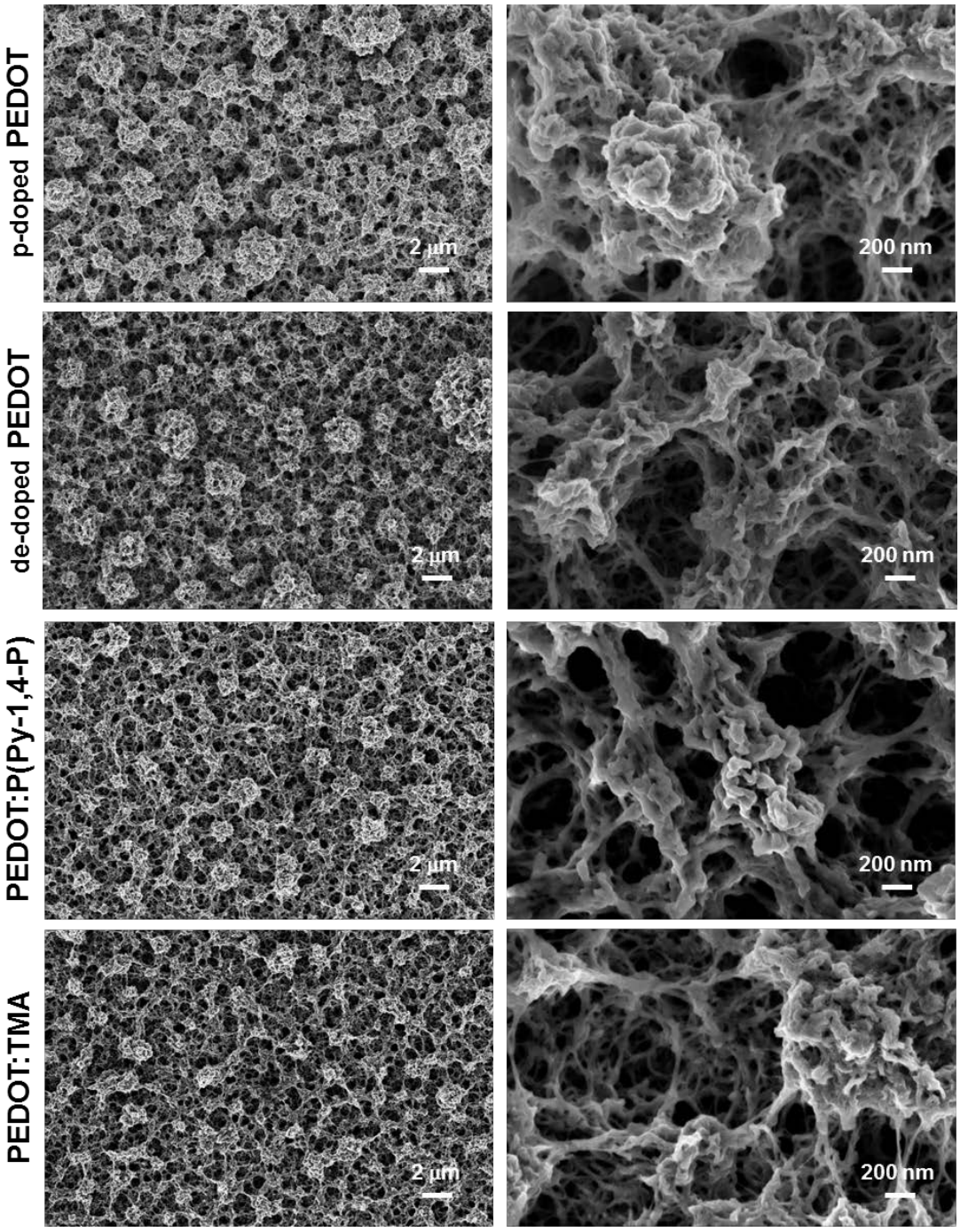
p-doped PEDOT
de-doped PEDOT
PEDOT:P(Py-1,4-P)
PEDOT:TMA
2 µm
200 nm

Figure 3

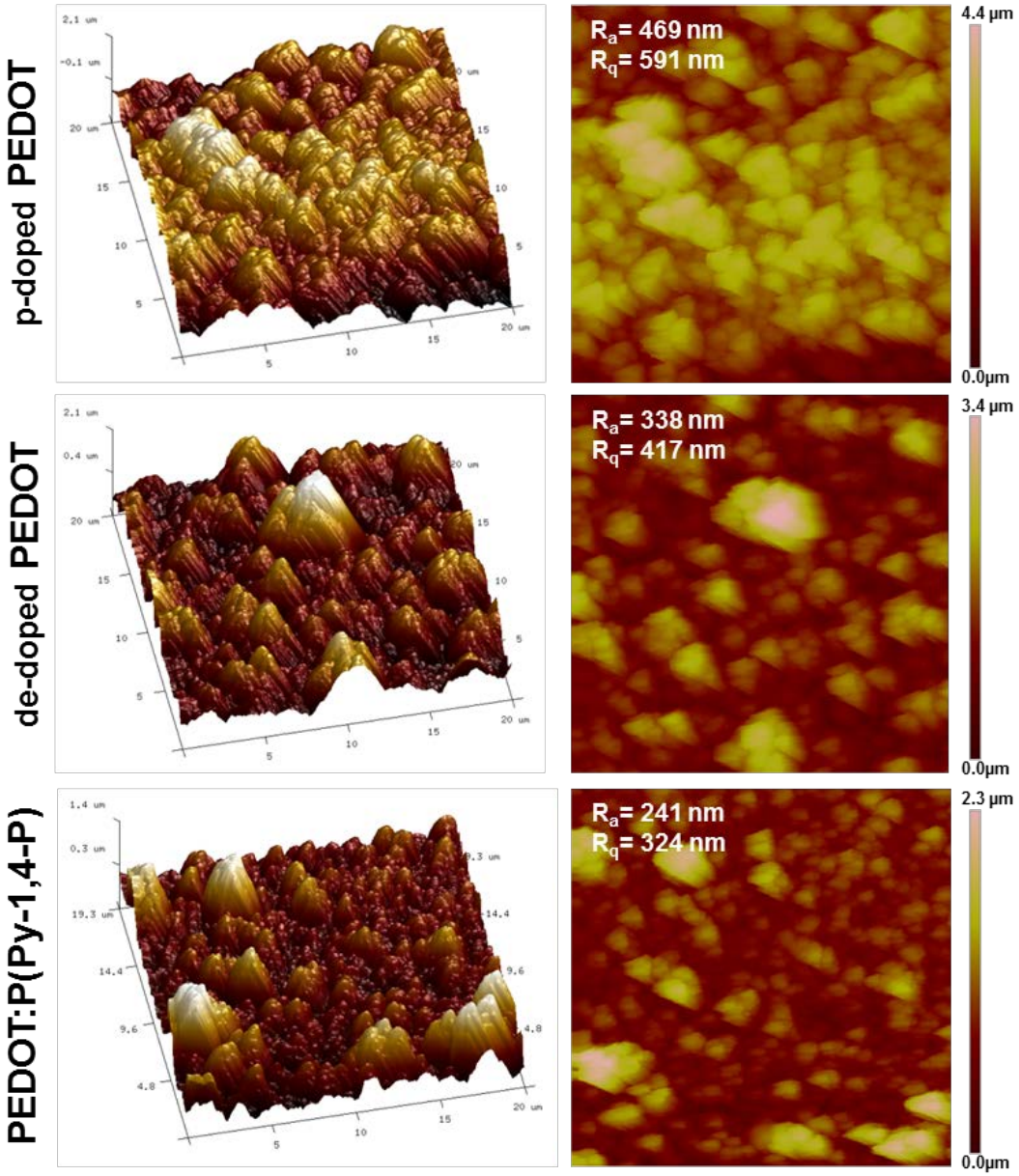
p-doped PEDOT
de-doped PEDOT
PEDOT:P(Py-1,4-P)
Ra= 469 nm
Rq= 591 nm
4.4 µm
0.0µm
Ra= 338 nm
Rq= 417 nm
3.4 µm
0.0µm
Ra= 241 nm
Rq= 324 nm
2.3 µm
0.0µm

Figure 4

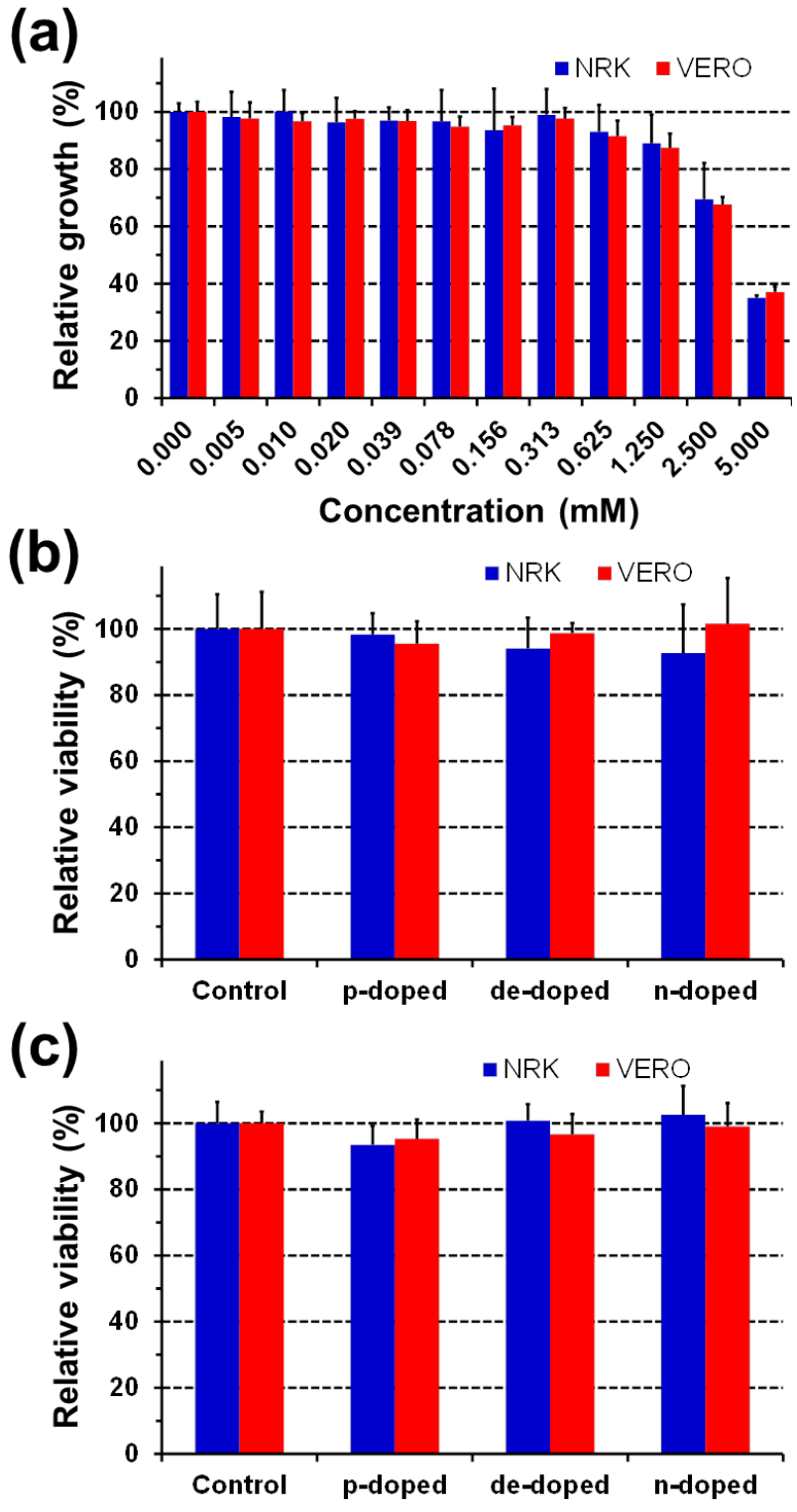
(a)
NRK
VERO
Relative growth (%)
100
80
60
40
20
0
0.000
0.005
0.010
0.020
0.039
0.078
0.156
0.313
0.625
1.250
2.500
5.000
Concentration (mM)
(b)
NRK
VERO
Relative viability (%)
100
80
60
40
20
0
Control
p-doped
de-doped
n-doped
(c)
NRK
VERO
Relative viability (%)
100
80
60
40
20
0
Control
p-doped
de-doped
n-doped

Figure 5

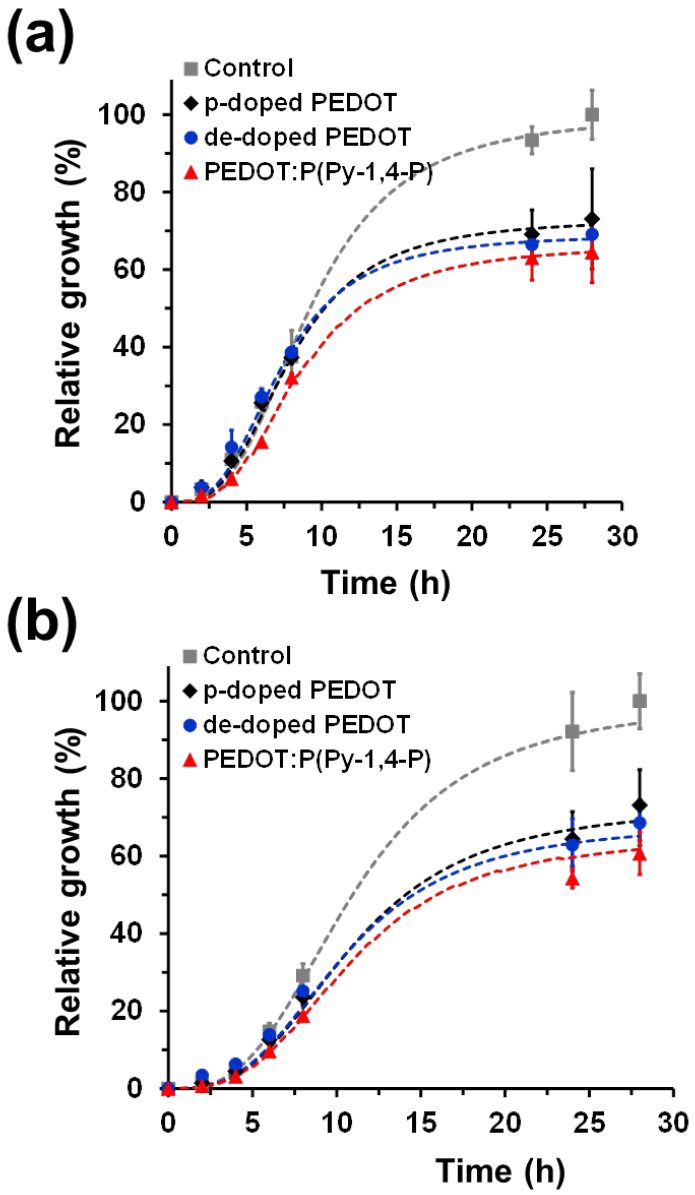
(a)
Control
p-doped PEDOT
de-doped PEDOT
PEDOT:P(Py-1,4-P)
Relative growth (%)
Time (h)
(b)
Control
p-doped PEDOT
de-doped PEDOT
PEDOT:P(Py-1,4-P)
Relative growth (%)
Time (h)

Figure 6

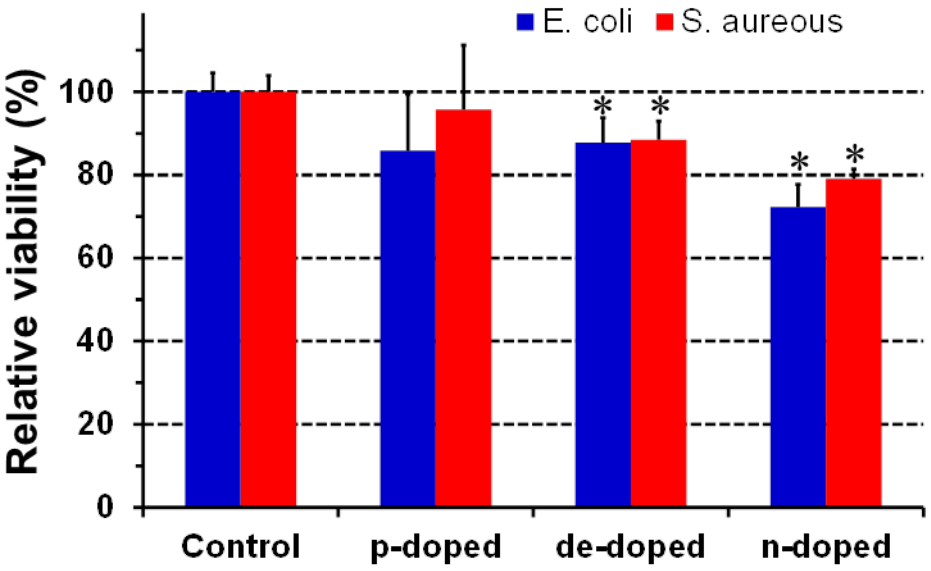
E. coli
S. aureous
Relative viability (%)
100
80
60
40
20
0
Control
p-doped
de-doped
n-doped
*
*
*
*

Figure 7

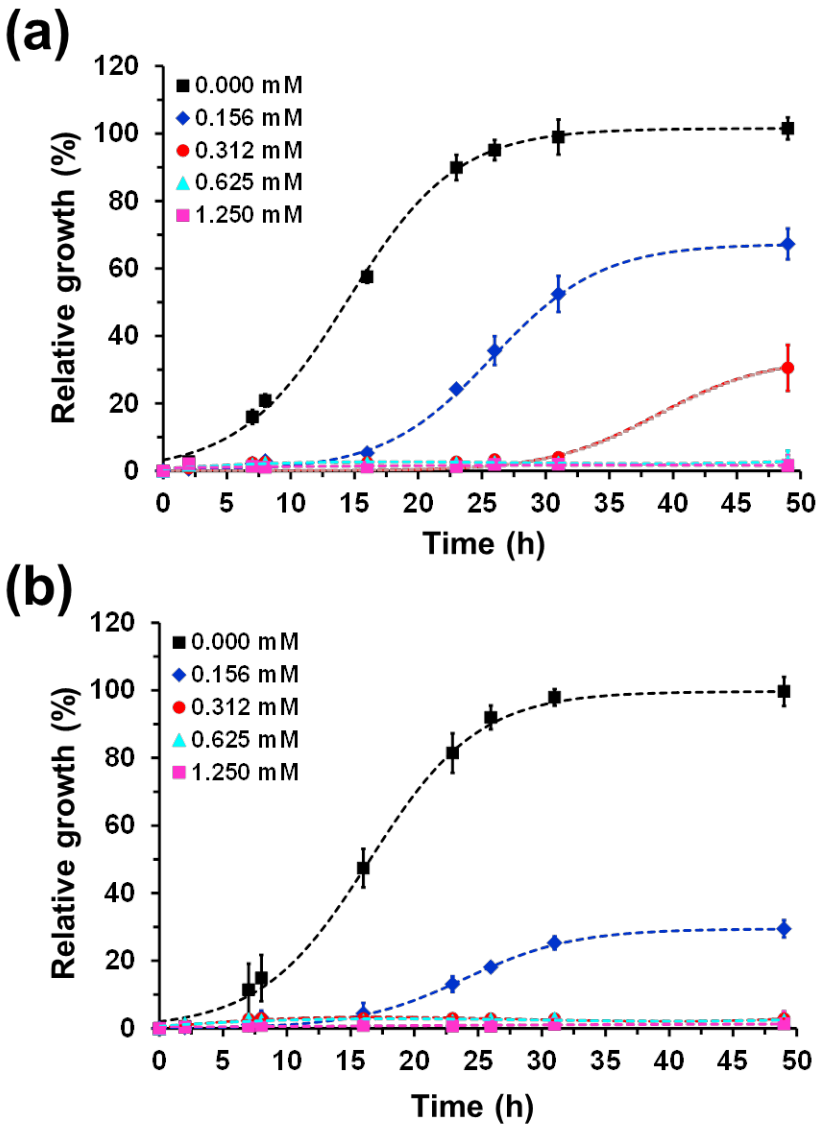
(a)
Relative growth (%)
Time (h)
0.000 mM
0.156 mM
0.312 mM
0.625 mM
1.250 mM
(b)
Relative growth (%)
Time (h)
0.000 mM
0.156 mM
0.312 mM
0.625 mM
1.250 mM

Figure 8

Graphical abstract